

UC Irvine

UC Irvine Previously Published Works

Title

Power optical Doppler tomography imaging of blood vessel in human skin and M-mode Doppler imaging of blood flow in chick chorioallantoic membrane

Permalink

<https://escholarship.org/uc/item/04v1p6sq>

Authors

Ren, Hongwu
Wang, Yimin
Nelson, J Stuart
et al.

Publication Date

2003-07-01

DOI

10.1117/12.479028

Copyright Information

This work is made available under the terms of a Creative Commons Attribution License, available at <https://creativecommons.org/licenses/by/4.0/>

Peer reviewed

Power optical Doppler tomography imaging of blood vessel in human skin and M-mode Doppler imaging of blood flow in chick chorioallantoic membrane

Hongwu Ren, Yimin Wang, J. Stuart Nelson, Zhongping Chen

Beckman Laser Institute and the Center for Biomedical Engineering,
University of California, Irvine, California 92612

ABSTRACT

We describe power optical Doppler tomography (ODT) imaging in phase-resolved optical coherence tomography (OCT) capable of providing the precise location of blood flow in human skin. The power Doppler signal is the squared amplitude of the Doppler signal. By properly setting the intensity threshold and priority displaying Doppler power in phase-resolved OCT, we obtained a Doppler power tomography image of the blood flow in human skin. Power Doppler tomography uses only the amplitude information, so it is not susceptible to aliasing and Doppler flow angle and provides more accurate and smooth imaging of the location of the blood vessels in human skin than Doppler velocimetry. We also modified the phase-resolved algorithm we published before and used it to do Doppler tomography and M-mode Doppler imaging. The dynamic blood flow in chick chorioallantoic membrane (CAM) was studied using M-mode Doppler imaging.

Keywords: Optical coherence tomography, phase-resolve optical Doppler tomography, power optical Doppler tomography, human skin, chick chorioallantoic membrane (CAM).

1. INTRODUCTION

Optical coherence tomography (OCT) is a new noninvasive imaging modality capable of probing cross-sectional images of tissue structure on a micrometer scale [1]. OCT is analogous to ultrasound imaging except that infrared light waves rather than acoustic waves are used. When imaging the eye, OCT does not need contact with the eye to get impedance matching as required for ultrasound. This noncontact nature is useful for eye imaging and eye disease diagnosis because it provides more comfortable imaging of the eye for patients. Moreover OCT can provide high-resolution imaging of the retinal tissue on the order of a few micrometers. Therefore OCT was successfully applied to ophthalmology for imaging and diagnosis of retinal disease clinically in the last decade. Recently, OCT has been applied to imaging subsurface structure and blood vessels in human skin and internal organs [2].

Optical Doppler tomography (ODT) is an extension of OCT for cross sectional imaging of tissue microstructure and blood flow simultaneously [3-16]. Recently phase-resolve ODT technique has been developed for imaging the phase change between A-line pairs when doing subsurface imaging to obtain additional physiologically important information [7-16]. The accurate determination of the location of blood perfusion is important especially in reconstruction of tissue microcirculation in three-dimension imaging [11].

2. METHODS

2.1 Phase-resolved ODT setup and trigger relationship

In this paper, we describe an algorithm to extract the power Doppler information and a new algorithm to extract velocity and standard deviation information in a phase-resolved ODT system. The algorithm given here is an extension of the

phase-resolved signal processing method developed in our laboratory. The flow images were obtained by processing the analytical interference fringe signals. The fiber-based phase-resolved ODT system is shown in Figure 1. A 1310 nm low coherent light source (AFC Technologies) with a FWHM bandwidth of 80 nm was used as the light source. Light was divided into sample and reference arms of the Michelson interferometer by a 3 dB 2x2 fiber coupler. In the reference arm, a rapid scanning optical delay (RSOD) line [17-18] works with only group-delay scanning at 500 Hz. An E-O modulator generates stable phase modulation at 500 kHz. A probe with a collimator and infinity-corrected objective driven by a translation stage is used in the sample arm. The fringe signals from the two polarization channels are detected by two photo-detectors, one connected to oscilloscope for monitoring and the other connected to preamplifier for processing. The detected signal is high pass filtered, amplified and digitized by a 12-bit analogue to digital conversion board (dual-channel, 5M samples/s per channel, National Instruments). The synchronizing time clock diagram is shown in Figure 2. The positive slope of the signal in channel 3 acts as a trigger to start the phase modulation signal generation and data acquisition. The negative slope acts as a trigger to stop the phase modulation signal generation

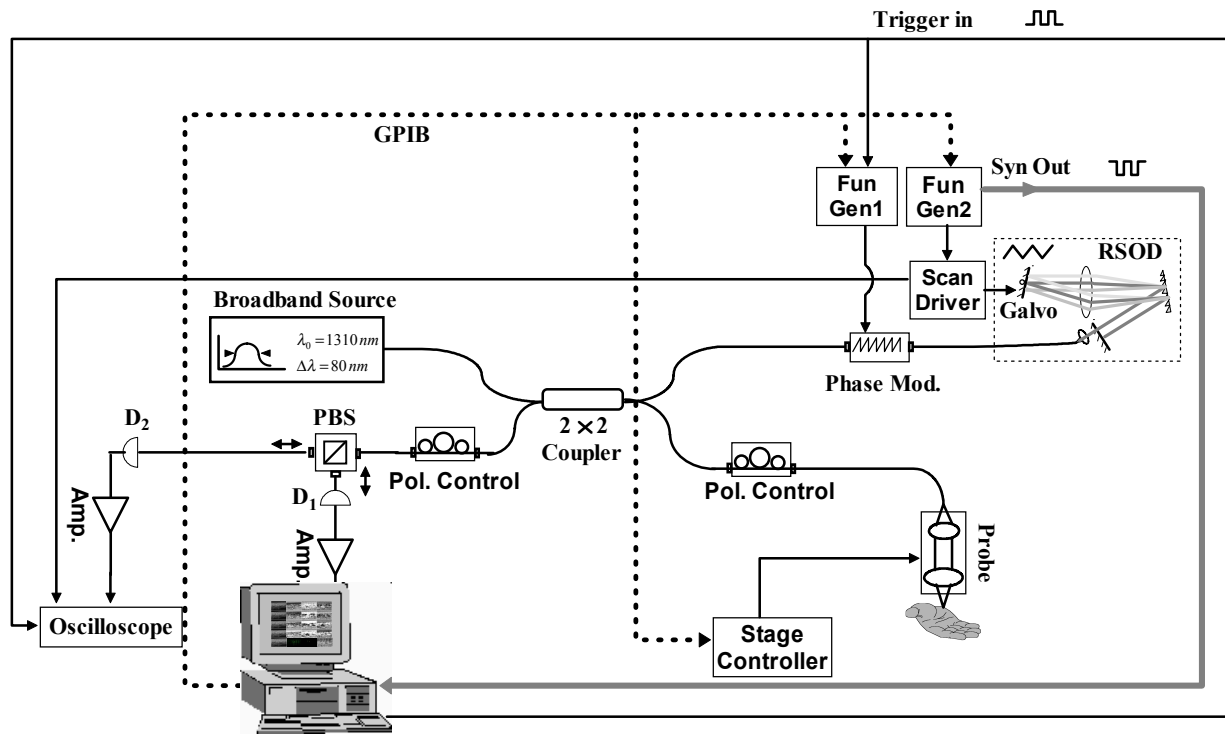


Figure 1. Fiber-based phase-resolved ODT system. Phase Mod.: Phase modulator, PBS: polarization beam splitter, Pol. Control: polarization controller, RSOD: rapid scanning optical delay line, D₁, D₂: detectors. Galvo: Galvanometer scanner, Fun Gen1, Fun Gen2: function generators, GPIB: general-purpose interface bus, Syn. Out: synchronizing signal of the driving signal for galvanometer scanner, which is from Fun Gen2, Trigger in: Trigger in signal to Fun Gen1, which is generated from the National Instruments (NI) DAQ board. Amp.: low noise preamplifier.

and data acquisition. Channel 1 is the triangle signal driving the galvanometer scanner. The driving signals for the phase modulator and galvanometer scanner are all generated by GPIB synthesis by two function generators. The translation stage moves continuously and goes one pixel in lateral direction accordingly when an integer number of A-line scans has finished.

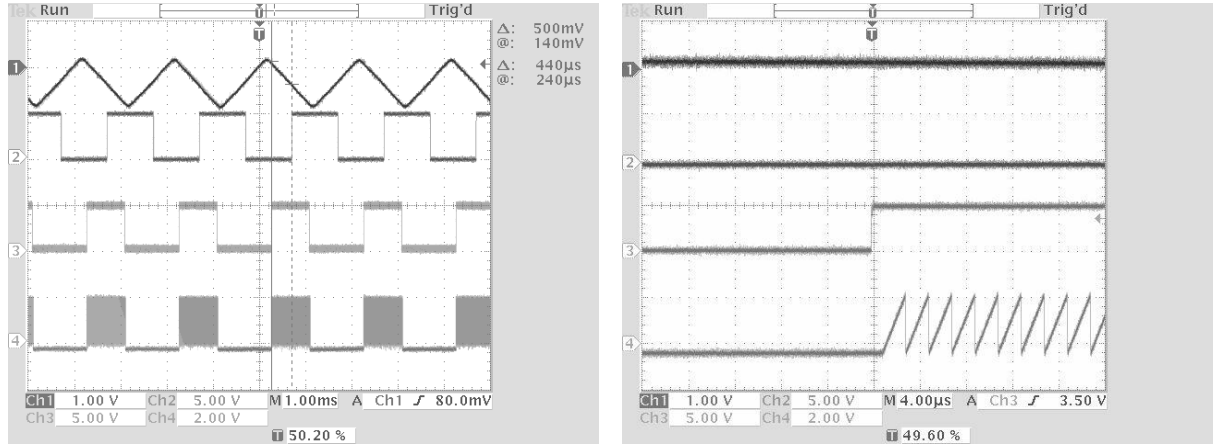
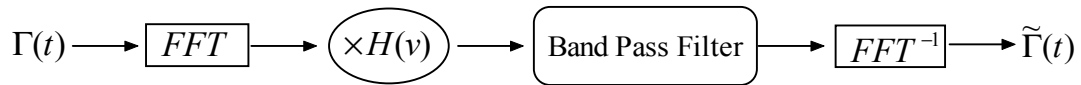


Figure. 2. Synchronizing time clock diagram for the phase-resolved ODT system. In Figure 2(1), Channel 1 is the triangle signal from the Function generator 2 to control the galvanometer scanning. Channel 2 is the synchronized output of the Channel 1 from Functional generator 2. Channel 3 is the signal generated by NI DAQ board through a digital shift of the positive slope of Channel 2 as shown in Figure 2(1) by a solid line and dotted line mark. The positive slope of channel 3 is obtained by shifting backward 440 microsecond of the positive slope of Channel 2. Channel 3 is used to trigger the phase modulation shown in Channel 4 and data acquisition. The 250 times zoom in of the phase modulation signal is shown in Figure 2(2).

2.2 Phase-resolved ODT signal processing

Because phase-resolved ODT imaging needs phase information, we obtain the complex analytical signal $\tilde{\Gamma}(t)$ of the interference fringe by the algorithm shown in the following block diagram [14,16]



where FFT denotes the fast Fourier transform, \times is a multiplying symbol, and $H(v)$ is the Heaviside function given by:

$$H(v) = \begin{cases} 0 & v < 0 \\ 1 & v \geq 0 \end{cases} \quad (1)$$

and FFT^{-1} denotes the inverse fast Fourier transform. The power ODT (P_n), Doppler flow velocity (f_n) and standard deviation (σ_n) values at the n th pixel can be calculated with complex analytical signals [16]:

$$P_n = \sum_{m=n-M/2}^{n+M/2} \sum_{j=1}^N \left| \tilde{\Gamma}_j(t_m) \cdot \tilde{\Gamma}_j^*(t_m) \right|^2 \quad (\text{threshold and priority}) \quad (2)$$

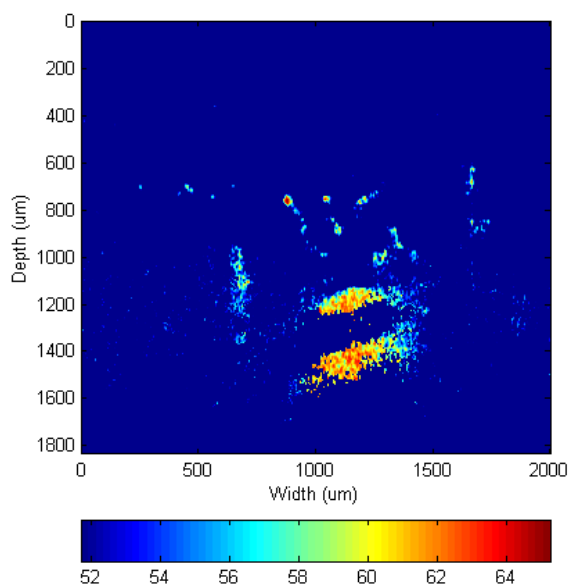
$$f_n = \frac{1}{2\pi T} \tan^{-1} \left(\frac{\text{Im} \left[\sum_{m=n-M/2}^{n+M/2} \sum_{j=1}^N \tilde{\Gamma}_j(t_m) \cdot \tilde{\Gamma}_{j+1}^*(t_m) \right]}{\text{Re} \left[\sum_{m=n-M/2}^{n+M/2} \sum_{j=1}^N \tilde{\Gamma}_j(t_m) \cdot \tilde{\Gamma}_{j+1}^*(t_m) \right]} \right) \quad (3)$$

$$\sigma_n^2 = \frac{1}{2\pi^2 T^2} \left(1 - \frac{\left| \sum_{m=n-M/2}^{n+M/2} \sum_{j=1}^N \tilde{\Gamma}_j(t_m) \cdot \tilde{\Gamma}_{j+1}^*(t_m) \right|}{\frac{1}{2} \sum_{m=n-M/2}^{n+M/2} \sum_{j=1}^N [\tilde{\Gamma}_j(t_m) \cdot \tilde{\Gamma}_j^*(t_m) + \tilde{\Gamma}_{j+1}(t_m) \cdot \tilde{\Gamma}_{j+1}^*(t_m)]} \right) \quad (4)$$

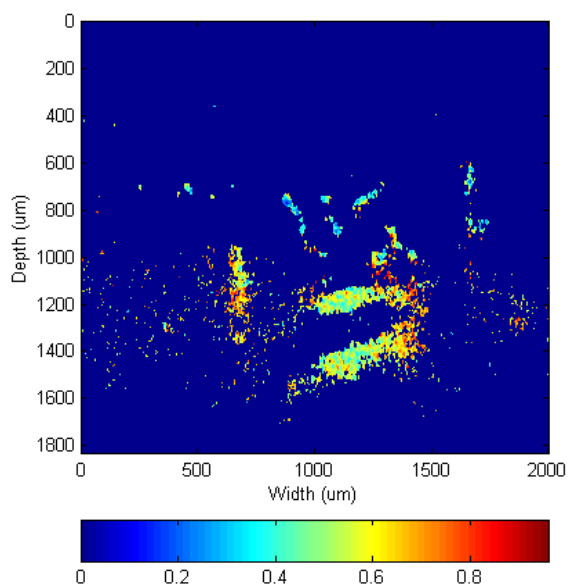
where M is an even number that determines the window size in the axial direction for each pixel, N is the number of A-line scanning for each pixel in the lateral direction. $\tilde{\Gamma}_j(t_m)$ and $\tilde{\Gamma}_j^*(t_m)$ are the complex signals at axial time t_m corresponding to the j th A-scan and its conjugate respectively, $\tilde{\Gamma}_{j+1}(t_m)$ and $\tilde{\Gamma}_{j+1}^*(t_m)$ are the complex signals at axial time t_m corresponding to the next A-scan and its conjugate, respectively, T is the time duration between A-scans, and M is an even number that denotes the window size in the axial direction for each pixel. Note that equation 5 is slightly different from our previously published work [9]. We replaced the term $\tilde{\Gamma}_j(t_m)\tilde{\Gamma}_j^*(t_m)$ with $1/2[\tilde{\Gamma}_j(t_m)\tilde{\Gamma}_j^*(t_m) + \tilde{\Gamma}_{j+1}(t_m)\tilde{\Gamma}_{j+1}^*(t_m)]$ to ensure non-negativity in the variance values. The modified algorithm shown in equations (3) and (4) also effectively reduces speckle noise. By properly setting the intensity threshold and priority of displaying with the help of the intensity and standard deviation images, we can obtain the power ODT image.

3. RESULTS

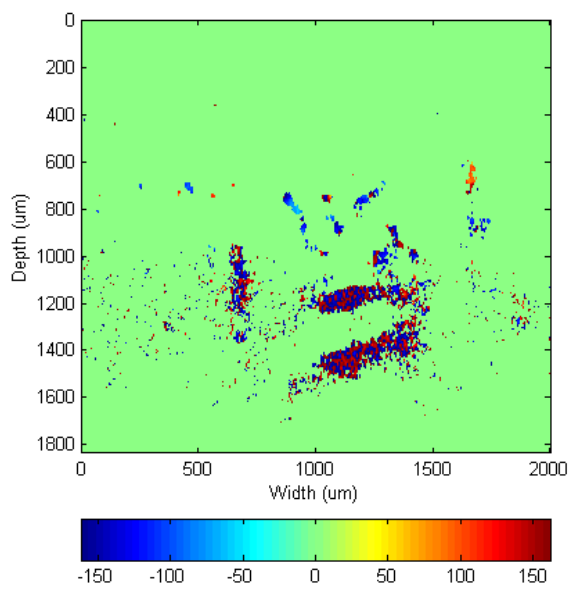
We have used our new phase-resolved algorithm system to perform in vivo imaging of a port wine stain birthmark in human skin. The power Doppler, blood flow velocity, and standard deviation images are shown in Figure 3. The imaged area is 1.8 x 2 mm. From these images we can see that the power ODT image gives clearer contour of the blood vessels in skin than the Doppler and standard deviation images. The power ODT image is not sensitive to speckle noise and other sources of phase noise. Because the statistical distribution of the phase of noise in phase-resolved OCT is uniform in the $[-\pi, \pi]$ range, the noise in ODT image is a diffuse random signal from negative to positive frequency. If not treated properly, noise can obscure the true flow velocity in ODT image. However, the amplitude of noise is assigned to a homogeneous background, therefore power ODT imaging gives a more uniform and smoother image of the location of the blood vessels in human skin than the Doppler velocity imaging at the cost of losing the velocity information. Another advantage of power ODT is that it is susceptible neither to Doppler flow angle because of using the amplitude information nor to the aliasing caused by 2π ambiguity [19] because the integral of the power is the same whether its phase wraps or not. Power ODT also can measure the distribution of the number of blood cells in a blood vessel because the power ODT signal is related to the number of blood cells in blood vessel. From Figure 3, we can see that in the large blood vessel, the power ODT signal is stronger, meaning more blood cells are in the vessel. The M-mode Doppler imaging of the dynamic blood flow in CAM is also investigated in this paper. The CAM was kept in room temperature, and was gradually deteriorating when the imaging was performed. The M-mode imaging of blood flow dynamics in CAM during its half-hour demise is shown in Figure 4. Every three minutes one M-mode imaging was performed.



(1) Power ODT image

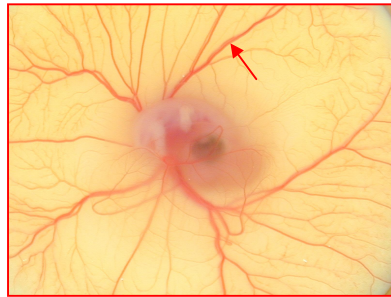


(2) Standard deviation image

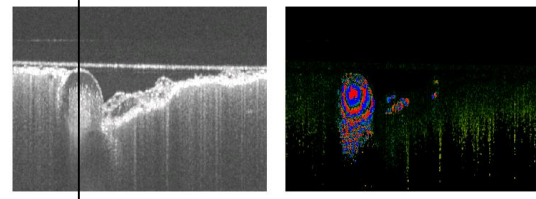


(3) ODT image

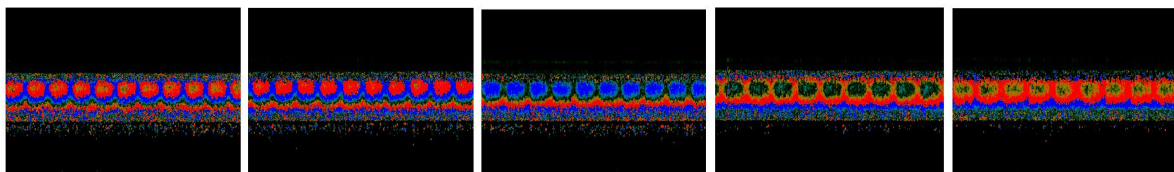
Figure3. Phase-resolved ODT imaging of the port wine stain in human skin. The imaged size is 1.8 x 2mm.



(1) CAM



(2) OCT and ODT image



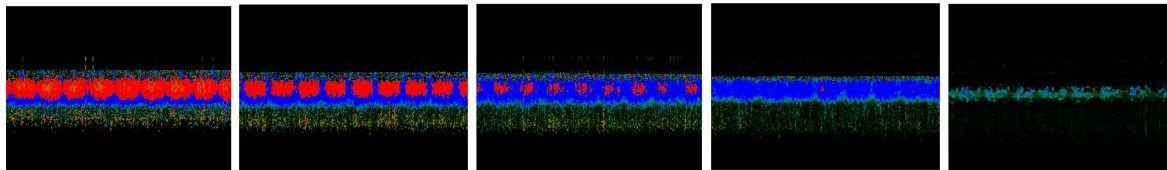
0 minute

3 minute

6 minute

9 minute

12 minute



15 minute

18 minute

21 minute

24 minute

27 minute

(3) M-mode Doppler image

Figure 4. M-mode Doppler imaging of blood flow in chick chorioallantoic membrane (CAM). OCT and ODT image size is 1.4×2 mm. A black line in OCT image marks the M-mode Doppler imaging position. For every M-mode Doppler image, the axial direction dimension is 1.4 mm and the temporal direction dimension is eight seconds. The red arrow in CAM image marked the position of M-mode Doppler imaging.

4. CONCLUSION

In summary, we have developed a modified phase-resolved algorithm for imaging of Doppler flow velocity, and standard deviation, which greatly reduces the influence of speckle noise. To the best of our knowledge, we did power ODT imaging of human skin for the first time. We have investigated the dynamics of blood flow in CAM by M-mode Doppler imaging. Power ODT and M-mode Doppler imaging will be a useful tool for dynamic imaging of the blood perfusion in biological tissues.

ACKNOWLEDGEMENTS

This work was supported by research grants awarded from the National Institutes of Health (EB-00293, RR-01192 and EB-00255) and National Science Foundation (BES-86924). Institutional support from the Air Force Office of Scientific Research (F49620-00-1-0371), and the Beckman Laser Institute Endowment is also gratefully acknowledged.

REFERENCES

1. D. Huang, E. A. Swanson, C. P. Lin, J. S. Schuman, W. G. Stinson, W. Chang, M. R. Hee, T. Flotte, K. Gregory, C. A. Puliafito, and J. G. Fujimoto, "Optical coherence tomography," *Science* 254, 1178-1181 (1991).
2. B. E. Bouma, and G. J. Tearney, "*Handbook of optical coherence tomography*," (Marcel Dekker, Inc. New York 2002).
3. Z. Chen, T. E. Milner, D. Dave, and J. S. Nelson, "Optical Doppler tomographic imaging of fluid flow velocity in highly scattering media," *Opt. Lett.*, 22, 64-66 (1997).
4. Z. Chen, T. E. Milner, S. Srinivas, X. Wang, A. Malekafzali, M. J. C. van Gemert, and J. S. Nelson, "Noninvasive imaging of *in vivo* blood flow velocity using optical Doppler tomography," *Opt. Lett.* 22, 1119-1121 (1997).
5. J. A. Izatt, M. D. Kulkarni, S. Yazdanfar, J. K. Barton, and A. J. Welch, " *In vivo* bidirectional color Doppler flow imaging of picoliter blood volumes using optical coherence tomography," *Opt. Lett.* 22, 1439-1441 (1997).
6. Z. Chen, T. E. Milner, X. J. Wang, S. Srinivas, and J. S. Nelson, "Optical Doppler tomography: Imaging *in vivo* blood dynamics following pharmacological intervention and photodynamic therapy," *Photochem. Photobiol.*, 67, 56-60 (1998).
7. Z. Chen, Y. Zhao, S. M. Srinivas, J. S. Nelson, N. Prakash, and R. D. Frostig, "Optical Doppler tomography," *IEEE J. Select. Topics in Quantum Electron.* 5, 1134-1141 (1999).
8. Y. Zhao, Z. Chen, C. Saxer, S. Xiang, J. F. de Boer, and J. S. Nelson, "Phase-resolved optical coherence tomography and optical Doppler tomography for imaging blood flow in human skin with fast scanning speed and high velocity sensitivity," *Opt. Lett.* 25, 114-116 (2000).
9. Y. Zhao, Z. Chen, C. Saxer, Q. Shen, S. Xiang, J. F. de Boer, and J. S. Nelson, "Doppler standard deviation imaging for clinical monitoring of *in vivo* human skin blood flow," *Opt. Lett.*, 25, 1358-1360 (2000).
10. J. S. Nelson, K.M. Kelly, Y. Zhao, and Z. Chen, "Imaging blood flow in human port-wine stain *in situ* and in real time using optical Doppler tomography," *Arch Dermatol*, 137, 741-744 (2001).
11. Y. Zhao, K. M. Brecke, H. Ren, Z. Ding, J.S. Nelson, and Z. Chen, "Three-dimensional reconstruction of *in vivo* blood vessels in human skin using phase-resolved optical Doppler tomography," *IEEE J. on Select. Topics in Quantum Electron.*, 7, 931-935 (2001).
12. V. Westphal, S. Yazdanfar, A. M. Rollins, and J. A. Izatt, "Real-time, high velocity-resolution color Doppler optical coherence tomography," *Opt. Lett.* 27, 34-36 (2002).
13. Y. Zhao, Z. Chen, Z. Ding, H. Ren, and J. S. Nelson, "Real-time phase-resolved functional optical coherence tomography by use of optical Hilbert transformation," *Opt. Lett.*, 27, 98-100 (2002).
14. Z. Ding, Y. Zhao, H. Ren, J. S. Nelson, and Z. Chen, "Real-time phase-resolved optical coherence tomography and optical Doppler tomography," *Opt. Express*, 10, 236-245 (2002).
15. H. Ren, K. M. Brecke, Z. Ding, Y. Zhao, J. S. Nelson, and Z. Chen, "Imaging and quantifying transverse flow velocity with the Doppler bandwidth in a phase-resolved functional optical coherence tomography," *Opt. Lett.*, 27, 409-411 (2002).
16. H. Ren, Z. Ding, Y. Zhao, J. S. Nelson, and Z. Chen, "Phase-resolved functional optical coherence tomography: simultaneous *in situ* imaging of the Stokes vectors, polarization diversity intensity, blood flow velocity, standard deviation, and birefringence in human skin," *Opt. Lett.* 27, 1702-1704 (2002).
17. G. J. Tearney, B. E. Bouma, and J. G. Fujimoto, "High-speed phase- and group-delay scanning with a grating-based phase control delay line," *Opt. Lett.* 22, 1811-1883 (1997).
18. M. Rollins, M. D. Kulkarni, S. Yazdanfar, R. Ung-arunyawee, and J. A. Izatt, "In vivo video rate optical coherence tomography," *Opt. Express*, 3, 219-229 (1998).
19. H. Ren, Z. Chen, K.M. Brecke, Z. Ding, Y. Zhao, and J. S. Nelson, "Imaging transverse flow velocity using spectral bandwidth of the Doppler frequency shift in phase-resolved ODT," *SPIE*, 4619, 137-144 (2002).